



THE UNITED STATES PATENT AND TRADEMARK OFFICE

Applicants: Paul R. Schimmel

Serial No: 08/249,689

Art Unit: 1805

Filed: May 26, 1994

Examiner: John Brusca

For: DESIGNING COMPOUNDS SPECIFICALLY INHIBITING RIBONUCLEIC  
ACID FUNCTION

Assistant Commissioner for Patents  
Washington, D.C. 20231

### TRANSMITTAL OF REPLY BRIEF

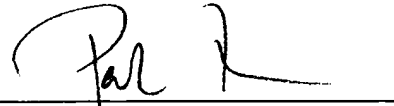
Sir:

In response to the Examiner's Answer, mailed April 17, 1996, which contained new grounds of rejection, enclosed is a Reply Brief, in triplicate. It is believed that no fee is required with this submission. However, should a fee be required, the

U.S.S.N.: 08/249,689  
Filed: May 26, 1994  
TRANSMITTAL OF REPLY BRIEF

Commissioner is hereby authorized to charge any additional fees to Deposit Account No. 01-2507. To facilitate this process, a duplicate of this Transmittal of Appeal Brief is enclosed.

Respectfully submitted,



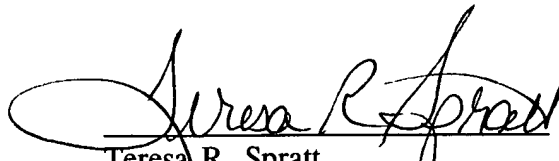
Patrea L. Pabst  
Reg. No. 31,284

Date: March 24, 1997

ARNALL GOLDEN & GREGORY  
2800 One Atlantic Center  
1201 West Peachtree Street  
Atlanta, Georgia 30309-3450  
(404) 873-8794  
(404) 873-8795 (fax)

**Certificate of Mailing under 37 CFR § 1.8(a)**

I hereby certify that this paper, along with any paper referred to as being attached or enclosed, is being deposited with the United States Postal Service on the date shown below with sufficient postage as first-class mail in an envelope addressed to the Assistant Commissioner for Patents, Washington, D.C. 20231.

  
Teresa R. Spratt

Date: March 24, 1997

IN THE UNITED STATES PATENT AND TRADEMARK OFFICE

Applicant: Paul R. Schiffmel



GP 1805  
#3  
1053  
RECEIVED

APR 25 1997

Serial No: 08/249,689

Art Unit: 1805

BOARD OF PATENT APPEALS  
AND INTERFERENCES

Filed: May 26, 1994

Examiner: John Brusca

For: DESIGNING COMPOUNDS SPECIFICALLY INHIBITING RIBONUCLEIC  
ACID FUNCTION

RECEIVED  
APR 23 1997  
GROUP 180

Assistant Commissioner for Patents  
Washington, D.C. 20231

**REPLY BRIEF**

Sir:

This Reply Brief is in response to the Examiner's Answer, mailed January 22, 1997, which contained new grounds of rejection and new points of argument.

**(1) RELATED APPEALS AND INTERFERENCES**

There is a related appeal in Application Serial No. 07/929,834. An Appeal Brief was mailed in this application on December 13, 1996. There are no other related appeals or interferences known to appellant, the undersigned, or appellant's assignee which directly affects, which would be directly affected by, or which would have a bearing on the Board's decision in this appeal.

**(2) ISSUES ON APPEAL**

The sole issue presented on appeal is that claims 1 and 3-21 are patentable under 35 U.S.C. § 112, first paragraph, since the specification, in combination with skill and knowledge in the art, enables those of skill in the art to make and use the claimed invention. Appellant is not appealing the merits of the provisional double patenting rejections which have been newly applied against claims 1, 3-6, 8-21 with respect to application 07/929,834. Rather, Appellant relies on the principle that a first conflicting application subject to a provisional double patenting rejection will be allowed to issue once the claims are otherwise allowable (MPEP § 804). When this occurs, Appellant intends to cancel conflicting claims in the second application.

**(3) RESPONSE TO NEW POINTS OF ARGUMENT**

The Examiner's Answer contained several new points of argument regarding the rejection under 35 U.S.C. § 112, first paragraph. Appellant responds to these points below.

**A. Requirement for X Ray Crystallography.**

The Examiner's Answer (page 6, lines 4-8) newly asserts that "[i]t is not predictable that the secondary and tertiary structure of the targeted RNA molecule could be determined by a skilled practitioner at the time of filing of the instant application because the determination of tertiary structure requires growth of a crystal of the RNA molecule that is suitable for X ray crystallography and growth of such crystals is unpredictable". No support

is provided for the allegation that the determination of tertiary structure requires growth of a crystal of the RNA molecule or X ray crystallography of the crystal. The statement appears to be mere opinion. Contrary to this statement, the structure of RNA molecules could and can be assessed using numerous techniques. As an illustration of this, Appellant submits with this Reply Brief a copy of Cantor and Schimmel, *Biophysical Chemistry* (W.H. Freeman and Co., San Francisco, 1980), pages 1291-1322. Cantor and Schimmel describe numerous techniques useful for determining the structure of an RNA molecule and specifically discuss the integration of information from various techniques to predict tertiary structures. Accordingly, the statement in the Examiner's Answer is clearly erroneous and cannot be used to support any aspect of the present rejection.

The Examiner's Answer newly cites Michel *et al.*, *Science* 273:1676-1677 (1996), which describes the determination of the structure of a 160 nucleotide domain of an RNA molecule by X ray crystallography. The Examiner's Answer notes (page 8, lines 10-12) that Michel *et al.* show "that it was not until 1996 that the *crystal* structure of an RNA molecule larger than tRNA was solved" (emphasis added). The significance of this to the current rejection is questioned since there is no requirement that the structure of the targeted RNA molecule be determined by crystallography (see discussion above). Appellant also notes that Michel *et al.* makes reference (page 1676, first column, lines 19-22) to the determination of the crystal structure of other large RNA molecules in prior years. Thus, the implication that determination of the crystal structure of RNA molecules, let alone determination of RNA

structure by other means (see Cantor and Schimmel), is unduly difficult is not supported by the cited evidence.

For reasons discussed above, Appellant asserts that the implication of the statement on page 17, lines 7-10, of the Examiner's Answer (i.e. that Michel et al. indicates that methods for determining the structure of RNA molecules were not well known at the time of filing) is insupportable.

**B. Unsupported Conclusions.**

The Examiner's Answer contains several new conclusion which are unsupported or insufficiently supported by evidence or reasoning. On page 9, lines 18-22, the Examiner's Answer concludes, without support, that "[i]t is unpredictable whether a site that when mutated inhibits the function of an RNA molecule will lead to the identification of the claimed critical site...such that when a compound specifically binds to the minor groove of the critical site, the function of the RNA molecule is inhibited". This appears to be mere opinion. Appellant notes that there are numerous examples of RNA molecules (some of which are cited in the specification) where a critical site determined by a loss of function mutation represents a site in the RNA molecule that cannot be altered, either by mutation or other alteration, without affecting the function of the RNA molecule. Appellant also notes that, contrary to the implication of the Examiner's Answer, it is reasonable to expect that a site in an RNA molecule which cause a loss of function when mutated would also be a site sensitive to other alterations such as binding of a compound.

On page 10, lines 6-11, the Examiner's Answer concludes, without support, that "it is unpredictable whether binding of a compound to an RNA molecule will inhibit the function of the RNA molecule because the inhibition of function of an RNA molecule requires that the compound both bind to the RNA molecule and inhibit a *functional interaction* between the RNA molecule and its normal cellular substrate" (emphasis added). Appellant initially points out that the claims do not require the inhibition of a functional interaction. Although it is not clear from the Examiner's Answer, it appears that this conclusion is based on the assumption that inhibition of the function of an RNA molecule can only be accomplished by specifically disrupting an interaction of that RNA molecule with some other molecule. In fact, binding of a compound to the target RNA molecule could, for example, merely disrupt the structure of the RNA molecule, the consequence of which would be a loss of function. Such a loss of function may result from a loss of interaction, but this is not required nor is it necessary to specifically design such an effect.

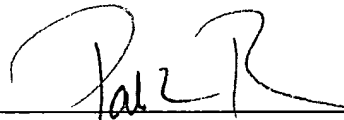
On page 18, lines 1-2, the Examiner's Answer states that "[w]eight is given to the claim of a pharmaceutical composition such that the specification must enable pharmaceutical use of the claimed composition" in support of requiring enablement of therapeutically efficacious use of the claimed compounds. Appellant strenuously disputes the propriety of this basis of rejection. Nowhere is there any legal support or justification for requiring enablement of what amounts to, at most, an intended use of the claimed compounds. Appellant submits that the "weight" given to such pharmaceutical compositions in the

U.S.S.N.: 08/249,689  
Filed: May 26, 1994  
REPLY BRIEF

Examiner's Answer is contrary to the requirements of law and cannot be used as a standard for judging enablement (see pages 9-11 in the Appeal Brief).

For the foregoing reasons, and for the reasons contained in the Appeal Brief mailed October 17, 1996, Appellant submits that the claims 1 and 3-21 are patentable.

Respectfully submitted,

  
\_\_\_\_\_  
Patrea L. Pabst  
Reg. No. 31,284

Date: March 24, 1997

ARNALL GOLDEN & GREGORY  
2800 One Atlantic Center  
1201 West Peachtree Street  
Atlanta, Georgia 30309-3450  
(404) 873-8794  
(404) 873-8795 (fax)



U.S.S.N.: 08/249,689  
Filed: May 26, 1994  
REPLY BRIEF

**Certificate of Mailing under 37 CFR § 1.8(a)**

I hereby certify that this paper, along with any paper referred to as being attached or enclosed, is being deposited with the United States Postal Service on the date shown below with sufficient postage as first-class mail in an envelope addressed to the Assistant Commissioner for Patents, Washington, D.C. 20231.

  
Teresa R. Spratt

Date: March 24, 1997

U.S.S.N.: 08/249,689  
Filed: May 26, 1994  
REPLY BRIEF

## **TABLE OF CONTENTS**

- (1) RELATED APPEALS AND INTERFERENCES**
- (2) ISSUES ON APPEAL**
- (3) RESPONSE TO NEW POINTS OF ARGUMENT**

Certificate of Mailing

Table of Contents

# BIOPHYSICAL CHEMISTRY

PART

III

## THE BEHAVIOR OF BIOLOGICAL MACROMOLECULES

**Charles R. Cantor**

COLUMBIA UNIVERSITY

**Paul R. Schimmel**

MASSACHUSETTS INSTITUTE OF TECHNOLOGY



W. H. FREEMAN AND COMPANY

San Francisco

Cover drawing after G. G. Hammes and C.-W. Wu,  
"Regulation of Enzyme Activity," *Science* 172:1205-1211  
at 1205. Copyright © 1971 by the American Association  
for the Advancement of Science.

*Sponsoring Editor:* Arthur C. Bartlett  
*Project Editor:* Pearl C. Vapnek  
*Manuscript Editor:* Lawrence W. McCombs  
*Designer:* Robert Ishi  
*Production Coordinator:* Linda Jupiter  
*Illustration Coordinator:* Cheryl Nufer  
*Artists:* Irving Geis and Eric Hieber  
*Compositor:* Syntax International  
*Printer and Binder:* R. R. Donnelley & Sons Company

Figures 16-11, 16-12, 16-14, 16-15b, 17-25,  
17-26, 24-16 copyright © 1980 by  
Irving Geis.

---

Library of Congress Cataloging in Publication Data

Cantor, Charles R. 1942-  
The behavior of biological macromolecules.

(Their Biophysical chemistry: pt. 3)

Includes bibliographies and index.

I. Macromolecules. I. Schimmel, Paul Reinhard,  
1940- joint author. II. Title  
QH345.C36 pt. 3 [QP801.P64] 574.19'283s 79-27860  
ISBN 0-7167-1191-5 [574.8'8]  
ISBN 0-7167-1192-3 pbk.

Copyright © 1980 by W. H. Freeman and Company

No part of this book may be reproduced by any mechanical,  
photographic, or electronic process, or in the form of a  
phonographic recording, nor may it be stored in a retrieval  
system, transmitted, or otherwise copied for public or private  
use, without written permission from the publisher.

Printed in the United States of America

9 8 7 6 5 4 3 2

## 24-2 TERTIARY STRUCTURE IN RNA

The supercoils we have discussed thus far are largely in the domain of tertiary rather than secondary structure. The conformational equilibria of supercoiling represent the coupling of both levels of structure. There also is clear evidence for the existence of tertiary structures in various RNA molecules. Here we briefly discuss some of the solution techniques that have revealed information about the structure of tRNA, the best-studied RNA. It is of particular interest to try to understand how a nucleic acid with a tertiary structure undergoes conformation changes, such as thermal unfolding.

### Evidence of tRNA tertiary structure in solution

The universality of the cloverleaf pattern of base pairing tRNA suggests that it surely must be a structural features of tRNAs. However, a number of lines of evidence indicate that the cloverleaf is not a complete description of the ordered structure of tRNA in aqueous solution. A cloverleaf such as that in Figure 24-13a (or Fig. 24-17) leads to a number of predictions inconsistent with experimental data. Hydrodynamically, a free cloverleaf either should behave like a flexible molecule or, if rigid, should resemble an oblate ellipsoid. However, hydrodynamic measurements are not in accord with such a structure.

Flexibility of tRNA (at least in a nanosecond time scale) is for the most part ruled out by fluorescence polarization measurements. These data yield a rotational relaxation time  $\tau_D$  of about 26 nsec. For a rigid spherical tRNA, one would predict that  $\tau_D$  should be only about 12 nsec. Flexibility can only lower this value, and oblate ellipsoids behave rotationally quite similarly to spheres. Thus the large measured  $\tau_D$  suggests that tRNA is more accurately modeled as a prolate shape, and that it must be fairly rigid. This conclusion is supported by a variety of other measurements, including intrinsic viscosity ( $\sim 6 \text{ cm}^3 \text{ g}^{-1}$ ) and sedimentation ( $\sim 4.2 \text{ S}$ ), both of which are inconsistent with spherical tRNA and argue instead for an elongated structure. Additional evidence comes from small-angle x-ray scattering, which is best fit by rigid elongated structures with lengths of 85 to 92 Å and widths and thicknesses of only 22 to 35 Å.

One of the strongest early indications of some kind of ordered tertiary structure in tRNA was the discovery of native and denatured forms. These two forms have relatively similar extents of base pairing as monitored spectroscopically. Therefore, the denatured form cannot be a random coil. The overall hydrodynamic properties of the two forms are quite different. Denatured forms can be created by removal of  $\text{Mg}^{2+}$  ions. They can be converted to native forms by incubation in the presence of magnesium ions. These observations indicate that divalent cations play a critical role in the stabilization of the native structure. The existence of denatured forms suggests that some kind of ordered folding of the cloverleaf exists in the native struc-

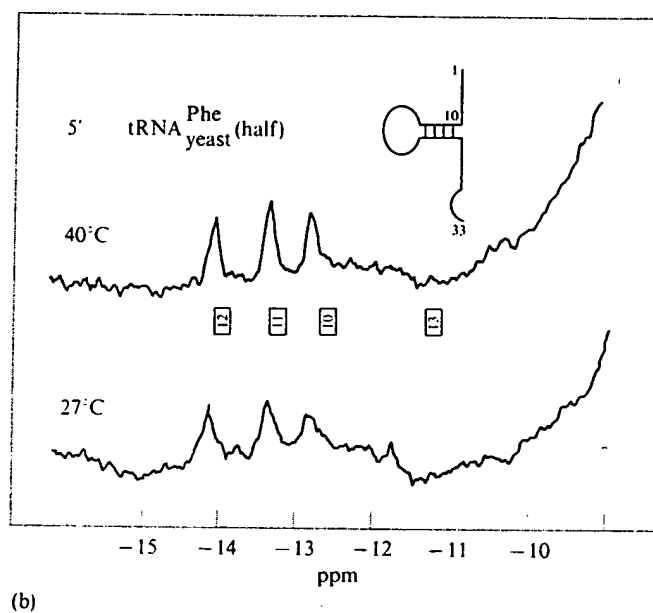
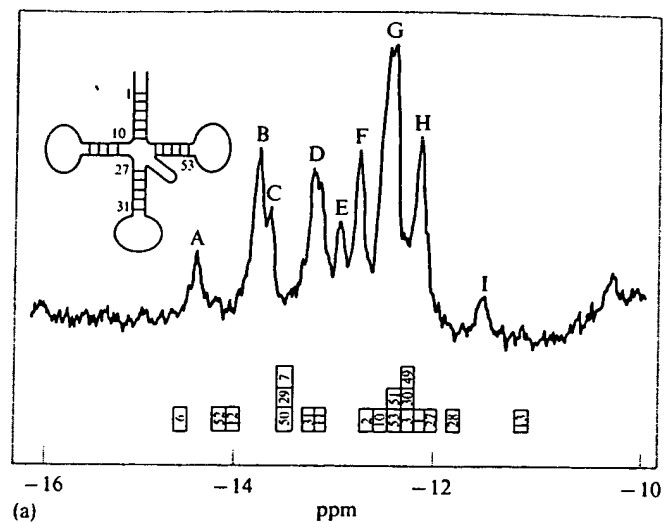


**Figure 24-13**

*Proton NMR spectra of tRNA at 300 MHz in H<sub>2</sub>O.* (a) Intact yeast tRNA<sup>Phe</sup> at two temperatures. The predicted locations of resonances from secondary-structure base pairs are shown in boxes. (b) A fragment of yeast tRNA<sup>Phe</sup>. [After D. R. Lightfoot et al., *J. Mol. Biol.* 78:71 (1973).]

ture; this folding is disrupted upon  $Mg^{2+}$  removal. After slight alterations in secondary structure, the conformation can rearrange to the denatured form. This form is metastable relative to the native form once  $Mg^{2+}$  is returned to the solution. However, the rate of interconversion can be quite slow.

Another set of experiments strongly indicating a tertiary structure involved chemical modification. If native tRNA were a simple cloverleaf one might expect two distinct classes of reactivity with reagents such as formaldehyde, kethoxal, and perphthalic acid that are known to modify base residues. Part of the tRNA should behave as a single strand, and the rest should behave as pure double-stranded duplex. However, experimental results showed that some residues predicted by the cloverleaf pattern to be single-stranded are inaccessible to reagents capable of reacting with isolated single strands (see Chapter 3). This result can be rationalized if, in native tRNA, the arms of the cloverleaf are folded up to make an ordered tertiary structure. Then experiments must be designed to examine the overall geometry of folding and to discover what specific interactions are responsible for the maintenance of the tertiary structure.

The pattern of chemical reactivity of native tRNA suggested that the anticodon loop and the 3'-end are relatively exposed, whereas other potentially single-stranded regions (such as the T $\psi$ C sequence) are not accessible. Without *a priori* knowledge of the tertiary structure, it is very difficult to explain the origin of particular alterations in reactivity. Furthermore, it is rather treacherous to attempt to deduce structural information from reactivity data alone, because very subtle alterations in structure can sometimes lead to large reactivity differences. However, the x-ray structural data currently available on yeast tRNA<sup>Phe</sup> (Chapter 3) do permit rationalization of much of the chemical modification pattern.

A major danger in chemical modification experiments is that structural alterations may be introduced in the process of forming covalent derivatives. Even when biological activity is maintained after the modification, one cannot be absolutely sure that the structure is identical. The advantage of physical studies in solution is that many of these entail no risk of structural alteration.

### Estimating tRNA base pairing in solution

One of the first goals in the study of an RNA structure is to estimate the fraction of bases involved in base pairing. When the optical methods outlined in Chapters 7 and 8 were applied to tRNA, it was found that simply modeling cloverleaf as a set of short duplexes and linear single strands cannot account for the observed CD or hypochromism. The discrepancies are in the direction expected if tRNA contains significantly more base pairing than is demanded by a simple cloverleaf model. This observation immediately suggested that the tRNA tertiary structure might be organized around a set of additional base pairs. However, there was no way to discern from optical studies which base pairs these might be.

Inspection of the available tRNA sequences revealed a few potential tertiary base pairs, but it did not indicate an obvious pattern containing a sufficient number of tertiary base pairs that could be common to all tRNAs in the same way as the universal cloverleaf applies to all. Furthermore, one could not rely on the quantitative accuracy of the optical analyses, because it was difficult to take into account any special optical interactions arising from particular loop conformations, unusual nucleotides, and any possible differences between the structure of double helices in folded tRNA and the structure of linear duplexes. Rapid tritium-exchange studies on tRNA were consistent with optical studies in pointing to more base-base interactions in the native structure than predicted by the cloverleaf model. However, once again, uncertainties in the interpretation of the data precluded their use for rigorous testing of various proposed tRNA models.

The fundamental problem with optical and rapid tritium-exchange studies is that they provide far too few pieces of information about the system. NMR is potentially vastly more powerful, because the individual contributions of each residue to the observed spectrum are (in principle) resolvable. Given the instruments presently available, most of the NMR spectrum of a tRNA is not easy to interpret. Resonances from bases stand out, but the rest is largely a blur. However, a striking exception involves the NH protons of hydrogen-bonded Urd and Guo and their strange-base analogs. As we have seen in earlier chapters, base pairing leads to large downfield shifts and, as a result, these resonances appear in the region of  $-11$  to  $-15$  ppm with respect to a dimethylsilapentane sulfonate (DSS) standard. In this region of the spectrum, only NH resonances are present. Because only a single proton is involved for each base pair, one can expect that a simple cloverleaf would show only 20 bands in the low-field spectral region. Even allowing for the possibility of a few tertiary base pairs, an experimental spectrum could be simple enough to analyze.

The low-field region of the NMR spectrum must be studied with  $H_2O$  as the solvent. Free NH protons exchange rapidly. In base-paired regions, the exchange is slowed (Chapter 22). When the exchange rate is significantly slower than the characteristic NMR times, individual NH proton resonances will be visible. However, actual experimental NMR measurement for a tRNA can take hours because of the extensive signal averaging required. If  $D_2O$  is used as a solvent, the resonances disappear once the NH protons exchange. In  $H_2O$ , exchange does not matter, as long as it is slow. There always are protons resident on the tRNA, and (on the average) each spends a long enough time bound to be detected before it is replaced with another. The difficulty in working with  $H_2O$  is that there is a large background of absorption due to the solvent, which has  $10^4$ - to  $10^5$ -fold greater proton concentration than an individual tRNA NH resonance. This background and the resonances of other tRNA protons are centered at frequencies away from the  $-11$  to  $-15$  ppm region, but they contribute to the baseline there and make quantitative measurements of the intensities of the NH proton resonances rather difficult.

Figure 24-13a shows a typical low-field tRNA NMR spectrum. Nine distinctly



resolved NH bands are visible in yeast tRNA<sup>Phe</sup>. Not all are of equal intensity, and this result suggests that some represent the contribution of two or more protons. Integration of the spectrum (compared with reference standards) originally suggested that  $18 \pm 1$  protons are being observed. Because the yeast tRNA<sup>Phe</sup> cloverleaf contains 20 base pairs (not counting a single G-U), it is a reasonable first assumption that all the resonances seen are due to base pairs forming the cloverleaf secondary structure.

### Assigning base-paired residues in NMR spectra of tRNA

To confirm the suggestion that the resonances in the range of  $-11$  to  $-15$  ppm are due to base pairs, it is necessary to assign the observed resonances to particular residues. A general approach to assignment is to study the NMR spectra of a vast array of model oligonucleotide duplexes. Then the NMR contribution of a base pair in a given sequence (say, the central A-U of ApUpG·CpApU) can be assigned by solving sets of simultaneous equations, much as we have done for optical and thermodynamic data (Chapters 22 and 23). In practice, NMR requires much larger samples of material than do these other techniques, and it has not yet been possible to accumulate a sufficient library of experimental reference spectra.

An alternative approach to assignment, facilitated by the much better resolution of the NMR technique, is to study specific fragments of the tRNA structure. Halves or quarters of a tRNA molecule should contain only 4 to 7 base pairs. Thus there is a reasonable chance that each NH resonance will be cleanly resolved from all the others. This prediction is confirmed very well, as shown for the spectrum of the 5'-half of yeast tRNA<sup>Phe</sup> in Figure 24-13b; this spectrum has only four low-field resonances. To assign these individual resonances, one resorts to theoretical calculations. An isolated single A-U or G-C NH hydrogen-bonded proton should have some particular fixed resonance frequency, shifted downfield from that of the free molecules by hydrogen bonding. Imbedding any base pair within a double helix will lead to additional shifts upfield, due to the ring currents of bases stacked above or below it. The ring-current magnetic anisotropy of each of the nucleic acid bases has been calculated from quantum mechanics, using some of the best available approximate wavefunctions.

In Chapter 22, we show how these anisotropies can be used to estimate the stacking geometry from the observed structure. For tRNA analysis, it was originally assumed that the geometry of the double-stranded regions is a normal RNA-11 helix. Then the anisotropies can be used to predict the resonance positions as a function of sequence. Because the intrinsic NMR intensities of the isolated base pairs in H<sub>2</sub>O are unknown, these values are allowed to be variables and are adjusted to give the best fit for a wide variety of data from tRNAs, fragments, and model oligonucleotide duplexes. The results are chemical shifts for isolated A-U ( $-14.8$  ppm), G-C ( $-13.7$  ppm), and A- $\psi$  ( $\sim -13.5$  ppm). The effect of stacking by neighboring base

pairs can only shift these resonances upfield. Thus, in early studies of tRNA, the approximation was made that all resonances downfield from  $-13.7$  ppm must belong to A-U base pairs.<sup>8</sup>

Table 24-1 shows the calculated upfield shifts for various nearest-neighbor base pairs. Two general features of these results can be noted. First, purine ring-current

Table 24-1

Calculated ring-current shifts for base pairs stacked adjacent to an existing base pair (see Note)

5'	3'	5'	3'
U = 0.0	A = 1.3	U = 0.0	A = 1.3
C = 0.0	G = 0.6	C = 0.0	G = 0.7
G = 0.0	C = 0.1	G = 0.0	C = 0.2
A = 0.1	U = 0.0	A = 0.0	U = 0.1
U-A		C-G	
U = 0.1	A = 0.0	U = 0.1	A = 0.0
C = 0.2	G = 0.0	C = 0.25	G = 0.0
G = 0.6	C = 0.0	G = 0.7	C = 0.0
A = 0.7	U = 0.0	A = 1.2	U = 0.0
3'	5'	3'	5'

NOTE: The existing base pair is shown at the center of the table. The upfield shifts are shown (in ppm) for each stacked base attached toward the end of the chain indicated at top and bottom of the table. For example, consider the duplex 5'UpC3'-5'GpA3'. The C is stacked toward the 3'-end of the chain from the U, so its effect is listed in the lower left-hand quadrant of the table: an upfield shift of 0.2 ppm. The G is stacked toward the 5'-end of the chain from the A, so its effect is read in the same quadrant as 0.0 ppm. Thus, the total effect is an upfield shift of 0.2 ppm in the U-A resonance. Similarly, the effects of the U and A bases on the G-C resonances are read in the upper righthand quadrant: the U has no effect, and the A produces an upfield shift of 1.3 ppm.

SOURCE: After R. Shulman et al., *J. Mol. Biol.* 78:57 (1973).

effects are much stronger than those of pyrimidines. Second, the 5'-linked base (3'-end base) on each strand is almost totally responsible for the shifts induced by the base pair. This second result is reasonable. In the RNA-11 helix, the 5'-linked-base is partially stacked over the N-H-N hydrogen bond of the adjacent base pair, whereas the 3'-linked base shows little overlap.

Certain assumptions are needed to use the results in Table 24-1. One must take it on faith that the actual helical parameters in the tRNA duplex regions are close to

<sup>8</sup> More recent studies have calculated the NMR of base-paired protons in yeast tRNA<sup>Phe</sup> using the molecular coordinates determined by x-ray crystallography. These calculated values fit the observed spectrum very well. However, they indicate that the isolated A-U pair should have a chemical shift of  $-14.3$  ppm, and that reverse Hoogsteen A-U base pairs may account for the very-low-field resonances (see Robillard et al., 1977). As a result, some of the assignments we describe for tRNA<sup>Phe</sup> may have to be revised.

those seen in fibers of long duplex RNAs. The base pairs at the ends of helices or at helix-loop interfaces are especially troublesome. It certainly is reasonable to guess that some helix distortion may occur at those places. Even more serious is the question of whether or not single-strand bases adjacent to the duplex stack on it and, if so, with what geometry. In general, stacking of single-strand residues adjacent to helices has been used and, for intact tRNA, it has been assumed that the CCA stem and T $\psi$ C stems are stacked to make a continuous helix. The spectra are sensitive to such assumptions and, therefore, tertiary-structure information is (in principle) present in the observed resonances. However, the sensitivity is not all that large, and the data must be better calibrated before they can be exploited.

Figure 24-13b shows proton assignments for the base pairs in the 5'-half of yeast tRNA<sup>Phe</sup>. Three sharp resonances are in good agreement with the predicted values. The fourth predicted resonance (for G<sup>22</sup>-C<sup>13</sup>) is observed not as a sharp band, but rather as a somewhat diffuse band at slightly lower field position than predicted. This result may be an indication that the structure is heterogeneous in the 5'-half; if so, G<sup>22</sup>-C<sup>13</sup> might be especially affected because it borders on a loop. The observed results can be explained by assuming that the orientation of A<sup>14</sup> in the loop is quite variable. In a similar way, assignments were made for the resonances of other tRNA fragments. Then, to treat the whole molecule, one assumes that no major shifts occur in the resonances of individual protons compared with their positions in the fragments. In fact, the predicted resonance positions do not align all that well with the observed peaks in the intact molecule, or even in the fragments (Fig. 24-13b). However, the assignments do fairly well explain the overall qualitative pattern of the spectrum.

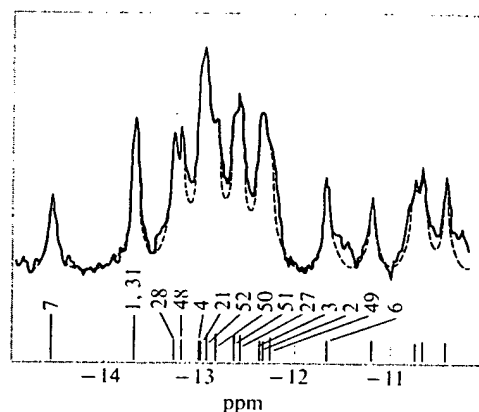
Improved analysis of NMR spectra of base-paired residues is possible by using a more empirical approach to band assignment. As we shall see, particular helical regions of a tRNA can sometimes be observed to melt individually. If these regions contain unique methylated bases, a clear assignment of the identity of the melting region often can be made by examining the methyl resonances. This assignment then assists the assignment of hydrogen-bonded proton bands because, in such a melting, all the bands due to one helical region should disappear simultaneously. Figure 24-14 shows an example of the extent to which secondary-structure resonances can be used to fit the NMR spectrum of a tRNA in which most of the bands have been assigned. Here a sample of yeast tRNA<sup>Asp</sup> was studied at 65°C, a temperature at which no tertiary structure exists. At this temperature, the pseudouridine stem is intact, and the anticodon and amino acid stems are partially melted. After the extent of melting of each region is taken into account, a computer is used to simulate the observed spectrum. Clearly, the agreement between calculation and experiment is excellent.

### Effect of tertiary structure on the NMR of tRNA

The success in analyzing the NMR of tRNA assures that, beyond reasonable doubt, the cloverleaf secondary structure is present in tRNA in aqueous solution. However, there are quite a few complications. For tRNA<sup>Phe</sup>, the original integration yielded

**Figure 24-14**

*NMR spectrum of yeast tRNA<sup>Asp</sup> at 65°C.*  
 The observed spectrum (solid curve) and  
 computer-simulated spectrum (dashed curve)  
 are shown. Numbered vertical bars indicate  
 positions assigned to individual residues.  
 [After G. T. Robillard et al., *Biochemistry*  
 15:1883 (1976).]

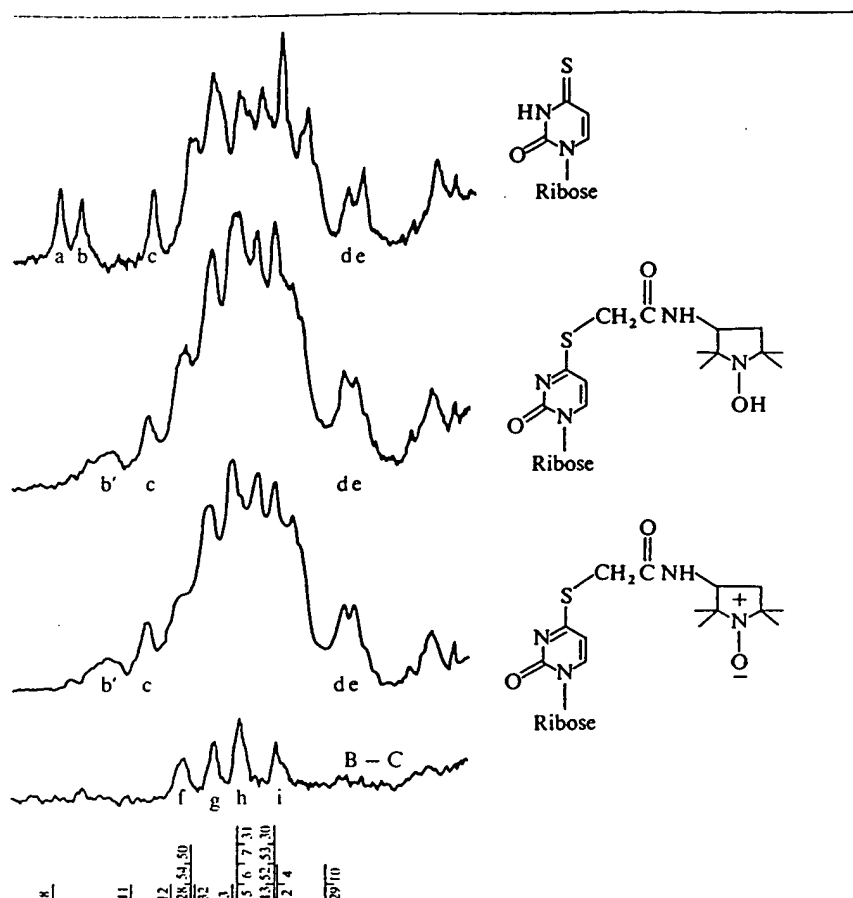


only  $18 \pm 1$  resonances, whereas the cloverleaf contains 20 normal base pairs. The detailed assignment located 19 resonances; one A-U appeared to be missing. Tentatively, this missing band was assigned to A<sup>5</sup>-U<sup>68</sup>, on the argument that the G-U may cause disruption of a relatively weak adjacent A-U. However, as we now know from the x-ray structure, tRNA contains many tertiary base pairs; these NH resonances should be visible in the NMR. More recent attempts to assign the NMR spectrum of tRNA have grappled with this problem.

A major factor that determines whether or not a resonance will be visible is the proton exchange rate. When the exchange rate approaches the NMR characteristic time for the two states of a proton, the resonance will broaden until, at a critical rate, the spectrum becomes infinitely broad and is unobservable. At even faster exchange rates for tRNA in H<sub>2</sub>O, the resonance remains invisible because its position is heavily weighted by the fraction of time that each proton spends as water rather than as base pair. Thus the resonance disappears into the huge water background. At present, it is not clear which types of secondary- or tertiary-structure resonances in an arbitrary conformation necessarily will have fast or slow exchange times. Thus, it now appears likely that some of the resonances originally assigned to secondary base pairs may actually belong to tertiary base pairs.

Improved normalization procedures have increased the number of protons that must be assigned to the integrated spectrum for most tRNAs. *E. coli* tRNA<sup>Met</sup> and tRNA<sup>Val</sup> show 27 and 26 low-field protons, respectively, whereas only 20 are demanded by a cloverleaf. Such results increase the difficulty of spectral assignment but are encouraging nonetheless, because solution of the assignment problem will make information on tertiary structure accessible directly from the NMR spectrum. Tertiary NH resonances are unlikely to be assigned from model-compound or oligonucleotide-duplex studies, because the tertiary interactions are absent in these systems. Instead, one must resort to perturbations of the intact tRNA.

Figure 24-15 shows an example of one very promising way to assign resonances in tRNA. A nitroxide free radical was covalently attached to the 4-thiouridine at



5

*R* spectra of *E. coli* tRNA<sup>Met</sup> at 220 MHz in H<sub>2</sub>O at 30°C. Curve A is the spectrum of native tRNA. Curve B is the spectrum of ascorbate-reduced tRNA spin-labeled at the 4-thiouridine in position 8. Curve C is the spectrum of tRNA spin-labeled at the 4-thiouridine in position 8. Curve D is the difference spectrum of curve C minus curve B. Predicted positions of secondary-structure resonances are shown at the bottom. [Daniel and M. Cohn, *Proc. Natl. Acad. Sci. USA* 72:2582 (1975).]

of *E. coli* tRNA<sup>Met</sup>. This paramagnetic species can broaden the resonances of protons located nearby in the structure. Any direct environmental alterations in the production of the nitroxide can be examined separately by reducing this derivative with ascorbate. Compared to unlabeled tRNA<sup>Met</sup>, the reduced spin-labeled derivative is missing a single resonance ("a" in Fig. 24-15), which therefore can be assigned to the proton normally hydrogen bonded between 4-thiouridine and the adjacent cytosine. In the difference spectrum caused by reduction of tRNA, if the difference spectrum is computed, four

discrete resonances appear. These can be assigned only tentatively at present. By combining expected chemical shifts and the known tRNA tertiary structure, one concludes that these four resonances apparently represent a G-C pair in the acceptor stem, a G-C pair in the dihydrouridine stem, and two G-C tertiary hydrogen bonds.

The NMR methods we have just described represent what is probably the most powerful solution technique currently available for the study of nucleic acid structure. They also are valuable in the dissection of individual steps in nucleic acid conformation changes, as we shall see shortly. NMR methods have been extended to examine slightly larger RNAs, such as 5 S rRNA. It seems likely that serious difficulties will arise in the study of RNAs larger than this. The number of base-pair resonances keeps increasing, and larger molecular weights almost inevitably lead to longer rotational correlation times, where dipolar broadening destroys the spectral resolution.

### Slow tritium exchange

The power of NMR is its ability to look at individual residues—if not one at a time, at least no more than a few at a time. Another technique with this potential is slow tritium exchange of C<sup>8</sup>-hydrogen (Chapter 22). Here we show the result of its application to tRNA by R. C. Gamble and P. R. Schimmel.

Any particular purine should exchange with tritium according to first-order kinetics:

$$\Delta(T)_i = \Delta(T)_{0i} e^{-t/\tau_i} \quad (24-6)$$

where  $i$  refers to the  $i$ th purine,  $\Delta(T)$  is the deviation from the equilibrium solvent tritium concentration at time  $t$ ,  $\Delta(T)_0$  is the deviation at time zero, and  $\tau$  is the decay time. In actual practice, exchange measurements are carried out for only a small fraction of one decay time. Therefore Equation 24-6 becomes, to a very good approximation,  $\Delta(T)_i = \Delta(T)_{0i}(1 - t/\tau_i)$ . For a polymer or oligomer containing multiple purines, the total amount of purine labeling will be

$$\Delta(T) = \sum_i \Delta(T)_{0i}(1 - t/\tau_i) \quad (24-7)$$

where the sum is over all purines in the molecule.

Equation 24-7 can be simplified by realizing that  $\Delta(T)_{0i}$  must be essentially the same for all purines. This value  $\Delta(T)_0$  will depend on the specific activity of the tritiated water used, on isotope effects that shift the final equilibrium extent of the exchange, and on the starting tritium content in each purine (which is zero for typical experimental arrangements). Then, for a polymer with  $N$  purines,

$$\Delta(T) = N \Delta(T)_0(1 - t/\bar{\tau}) \quad (24-8)$$

where  $\bar{\tau}$ , the average exchange time, is given by

$$1/\bar{\tau} = N^{-1} \sum_i (1/\tau_i) \quad (24-9)$$

If the total exchange into an oligomer or polymer is measured,  $\bar{\tau}$  can be computed.

To highlight the effects of secondary or tertiary structure on the exchange, one should compare the results either with monomer exchange rates ( $\tau_A^0$  and  $\tau_G^0$ ) or with the rates of a pure single-stranded oligomer. If the former comparison is used, one can compute an expected single-strand exchange time  $\bar{\tau}_0$  from Equation 24-9 as

$$1/\bar{\tau}_0 = \chi_A/\tau_A^0 + \chi_G/\tau_G^0 \quad (24-10)$$

where  $\chi_A$  and  $\chi_G$  are the mole fractions of these residues in the sample. Results usually are expressed as the retardation of tritium exchange:

$$R = \bar{\tau}/\bar{\tau}_0 \quad (24-11)$$

In the use of Equation 24-11,  $\bar{\tau}$  always is the measured time for a particular structure but, depending on the reference method used,  $\bar{\tau}_0$  either is calculated by Equation 24-10 or is measured.

Two levels of resolution can be employed for tritium-exchange studies on tRNA. Easiest experimentally is to exchange tritium in an intact tRNA and then to cool and to carry out a total enzymatic digestion with an endonuclease such as  $T_1$  RNase, which cleaves specifically after guanine residues. This procedure provides a distinct nonoverlapping set of fragments, which are separated in so far as possible by chromatography or electrophoresis. Then radioactive counting on each fragment permits calculation of its  $\bar{\tau}$ . Even more informative in many cases is further digestion of each separated oligonucleotide fragment into mononucleotides prior to tritium analysis. In this way, the exchange into adenine and guanine residues can be determined separately, and any effects of pyrimidine exchange can be corrected for. In principle, it should be possible to carry the method even further. The use of more than one specific nuclease would permit separate monitoring of the tritium exchange into each individual purine.

Figure 24-16 shows some quite informative results from slow tritium exchange on yeast tRNA<sup>phe</sup>. The general agreement with the known crystal structure of this tRNA is excellent. Regions that definitely are single-stranded (such as the CCA terminus and the anticodon loop) have values of  $R$  less than 5, indicating that exchange is only slightly impeded by conformation. Double-strand tRNA purines show values of  $R$  greater than 15, which is expected because purines in pure double-stranded RNAs have similar values. A few specific residues that are single-stranded in the cloverleaf representation still show  $R$  values between 15 and 30. Among these are the residues A<sup>14</sup>, G<sup>15</sup>, and G<sup>57</sup>. These results are reasonable because these

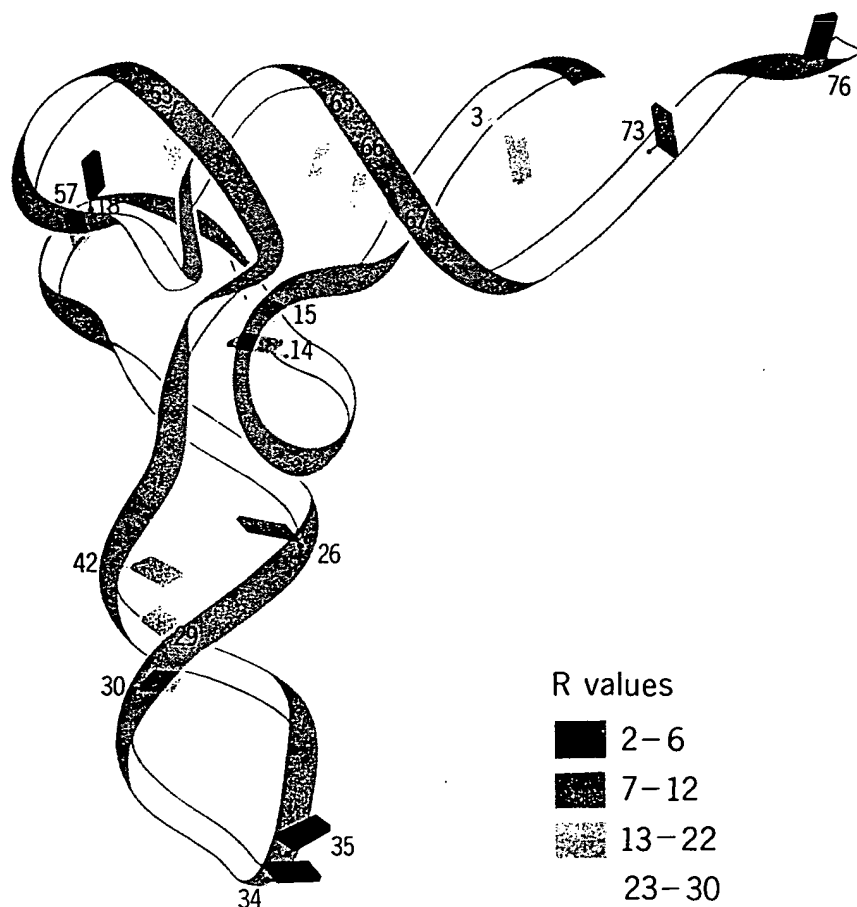


Figure 24-16

*Kinetics of purine C<sup>8</sup>-hydrogen tritium exchange in yeast tRNA<sup>Phe</sup>, superimposed on a schematic drawing of the tertiary structure of this tRNA. Shown is each of the purines for which exchange data at 37°C are currently available. The color indicates the relative exchange rate at each position. Except for residue G<sup>18</sup>, all purines implicated in secondary or tertiary structure in the crystal show substantially reduced exchange rates. [Drawing by Irving Geis.]*



residues either are involved in tertiary-structure base pairing, or else at least appear to be tightly folded into the structure (Fig. 24-16). The only real discrepancy is the exchange rate of G<sup>18</sup>, whose *R* value of only 4 suggests that it is exposed or uninvolved in tertiary interactions. Perhaps, at 37°C (the temperature at which tritium-exchange measurements are carried out), some tertiary features seen in the crystal at low temperature are melted, or at least are weakened sufficiently to show rapid tritium exchange.

### Oligonucleotide binding

A third high-resolution technique for studying the structure of tRNA in solution is the oligonucleotide-binding method. This method is particularly suited for identifying exposed single-stranded residues. Oligonucleotides are selected to be complementary to short stretches of the known tRNA sequence. Their binding strength to the RNA then is measured by equilibrium dialysis. A high concentration of tRNA is placed in a chamber on one side of a membrane impermeable to tRNA but permeable to smaller molecules. Radioactive oligonucleotide at low concentration is placed in a chamber of equal volume on the other side of the membrane. At equilibrium, the concentration of unbound oligonucleotide must be the same in the two chambers. Let  $K_b$  be the binding constant for an oligonucleotide to a single site in the tRNA:

$$K_b = (\text{Oligo} \cdot \text{tRNA}) / (\text{Oligo})(\text{tRNA}) \quad (24-12)$$

Because tRNA is present in great excess, its free concentration can be taken as equal to the input concentration. Then, just by rearranging Equation 24-12, we have the equilibrium ratio of total oligomer in the two dialysis chambers:

$$r_d = [(\text{Oligo} \cdot \text{tRNA}) + (\text{Oligo})] / (\text{Oligo}) = 1 + K_b(\text{tRNA}) \quad (24-13)$$

Thus,  $K_b$  can be measured in a very simple way.

If there are multiple binding sites, indexed by *i*, then we have the following expression for  $r_d$  in the limit of tRNA excess:

$$r_d = 1 + \sum_{i=1}^n K_{bi}(\text{tRNA}) \quad (24-14a)$$

If all *n* sites have comparable binding constants, then

$$r_d \cong 1 + nK_b(\text{tRNA}) \quad (24-14b)$$

The result is simply to increase the apparent value of  $K_b$  in Equation 24-13; therefore, the presence of multiple sites cannot be detected in the limit of tRNA excess. However, from known tRNA sequences, it is rare that more than two sites exist complementary

to a given trimer, and rare that there are even two sites complementary to any particular tetramer. So, if one restricts attention to only large differences in apparent  $K_b$  for different oligonucleotides, the effect of numbers of binding sites on an interpretation of data will not be that consequential. How long should the oligonucleotides used for this purpose be? It is comparatively difficult to synthesize compounds of length four or more, and the number of specific oligonucleotides of length  $n$  increases as  $4^n$ . However, longer oligonucleotides have greater specificity and higher binding constants. In practice, a common compromise is to work with lengths of three and four.

An effective strategy is to compare the binding strength of a tetramer with the strengths of its two constituent trimers. Consider a tRNA containing the sequence 3'...UpCpGpC...5'. We compare the binding strength to this sequence of the tetramer 5'ApGpCpG3' versus the trimers ApGpC and GpCpG. If all four bases on the tRNA are in a single-stranded section available for simultaneous binding to the four bases of the tetramer AGCG, its association constant should be much larger than that of either trimer. There will be three double-strand stacking interactions in the tetramer complex, but only two for each of the trimers. You can estimate from Table 23-4 that the third stacking interaction is worth about  $-3 \text{ kcal mole}^{-1}$  in free energy on the average; this would correspond to an increase in  $K_b$  by a factor of  $\exp(3,000/RT)$ , or 148 at 25°C. If the complementary tRNA sequence is in a loop, the extra tetramer-binding affinity is slightly more difficult to estimate, but it still should be significant. If only three tRNA bases of the four are accessible simultaneously, then  $K_b$  for the tetramer should be quite similar to one of the trimer values. (One might expect the tetramer  $K_b$  to be up to 10-fold stronger than the trimer  $K_b$  if the extra base is able to stack at the end of the duplex.) If both sets of three tRNA bases are separately available and nonoverlapping, the tRNA site just corresponds to two independent trimer sites; the  $K_b$  for the tetramer will be twice the trimer value.

In a similar way, dimer binding can be used as a reference state for trimers. This approach generally is not as useful, because many dimers bind too weakly to be studied. An important set of controls for all experiments is to use oligomers for which the complementary sequence does not exist anywhere on the RNA. These almost inevitably are found to bind much more weakly than any correctly complementary oligomers.

### Results of oligonucleotide-binding studies

O. Uhlenbeck has carried out an extensive set of oligonucleotide-binding studies on *E. coli* tRNA<sup>Tyr</sup>. Although the three-dimensional structure of this tRNA is not yet known, we summarize the results here anyway to demonstrate the power of this technique. Figure 24-17 shows the sequence of the tRNA folded as a cloverleaf. Uhlenbeck studied the binding of 63 of the 64 possible trinucleotides to tRNA<sup>Tyr</sup>, and 24 of these showed binding constants above the level set by the background in

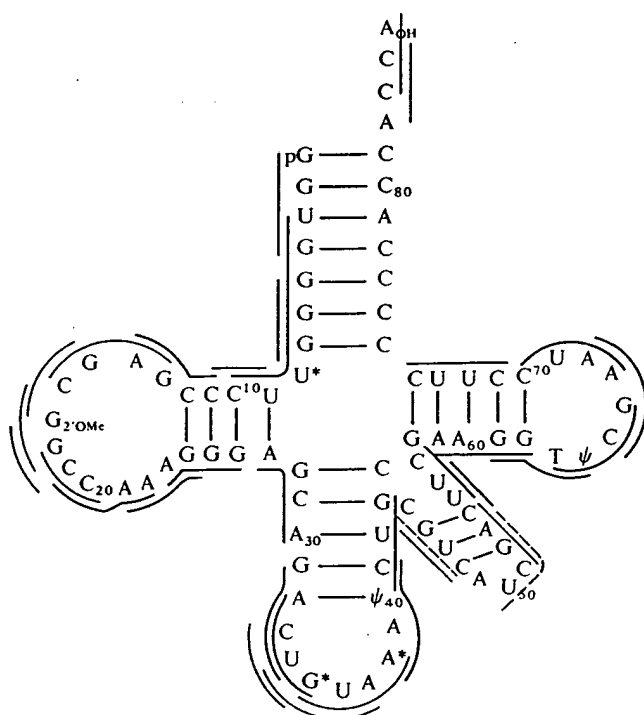


**Figure 24-17**

*Oligonucleotide binding to tRNA.* This diagram summarizes part of the results of Uhlenbeck's study of *E. coli* tRNA<sup>Tyr</sup>. Solid colored lines show complementary oligomers that bind strongly to the native tRNA. Dashed bars represent intermediate binding strengths. Black bars denote oligomers that do not bind significantly.

the experiments. Then, some 70 selected tetramers out of 256 possible were tested. Only 13 of these 70 tetramers showed binding constants larger than twice the sum of the constants of their constituent trimers (Table 24-2).

Tetramer-binding enhancements ranged from just barely twice the constituent trimer constants to a 50-fold increase for the two tetramers UACA and UAUA complementary to the anticodon of the tRNA. Note that the strong binding of UAUA implies that the G-U pair predicted by the wobble hypothesis for the third position of the codon-anticodon complex may actually contribute to the stability of duplex formation.

When all the trimer and tetramer results are compared, the results are consistent with the availability for oligomer binding of only four discrete regions of the tRNA: the 3'-ACCA sequence, the end of the extra loop, the anticodon, and part of the dihydrouridine loop (Fig. 24-17). The few oligomer-binding data that do not fit this pattern can be rationalized. For example, trimers containing a GpG sequence

Table 24-2

Tetranucleotides that bind to tRNA<sup>Tyr</sup> with  $K_b \geq 2K_{tri}$  (see Note)

Tetranucleotide	$K_b$ (M <sup>-1</sup> )	$K_{tri}$ (M <sup>-1</sup> )	Control tetramers	Classification
UACA	100,000	1,800	UACG, UGCA	+
UAUA	37,000	600	UAUG, UGUA	+
UUAC	5,300	900	UUAU, UUAG	+
ACAG	3,800	1,900	ACAA, UCAG	I
GCUC	22,000	1,800	GCUA, GUCC	+
CCGC	12,500	3,900	CUGC	I
GCCG	16,600	4,500	—	I
GUCG	8,700	1,400	GUCC, UUCG	+
GAUG	4,700	600	UAUG, GAAG	+
GUCU	5,000	900	GUCC	+
GACG	4,700	2,000	UACG, GAAG	I
UCGA	3,300	1,400	UGCA	I
UGUG	4,200	1,500	—	I

NOTE:  $K_{tri}$  is the sum of the  $K_b$  values of adjacent constituent trimers of the given tetramer. The  $K_b$  values are given for those tetramers in which all four bases are judged to bind simultaneously to tRNA<sup>Tyr</sup> (those with  $K_b \geq 2K_{tri}$ ). The control tetramers are those of similar sequence and composition that do not bind to tRNA<sup>Tyr</sup>. The binding tetramers are classified in the final column as strong binding (+) or intermediate binding (I).

SOURCE: After O. Uhlenbeck, *J. Mol. Biol.* 65:25 (1972).

appear to bind significantly to CC sequences, regardless of whether or not neighboring base pairs can form. This binding is reasonable in view of the fact that GG-CC is by far the strongest duplex interaction (Table 23-4).

Additional information is available from oligonucleotide competition binding. For example, suppose that a weakly binding, unlabeled trimer is added in a significant amount relative to the tRNA present, with total tRNA still in excess over a labeled oligonucleotide. Then the effect of the competitor is to complex part of the tRNA, depending on its binding constant,<sup>§</sup>

$$K_c = (\text{Compet} \cdot \text{tRNA}) / (\text{Compet})(\text{tRNA}) \quad (24-15)$$

This competitive binding reduces the available concentration of tRNA left to bind to the labeled oligomer by a factor of

$$(\text{tRNA}) / [(\text{tRNA}) + (\text{Compet} \cdot \text{tRNA})] = [K_c(\text{Compet}) + 1]^{-1} \quad (24-16)$$

<sup>§</sup> The complication that the labeled and unlabeled oligonucleotides might interact directly to form a complex is unimportant, so long as this complex is dialyzable.

**Table 24-3**  
Competition between oligonucleotides that bind to tRNA<sup>Tyr</sup>

Oligomer	Competitor	$K_b$ (M <sup>-1</sup> )	$K_{obs}$ (M <sup>-1</sup> )	$K_c$ (M <sup>-1</sup> )
GGC	GGC	102,000	13,000	114,000
GGU	GGC	48,000	46,000	670
UGG	GGC	9,000	9,300	0
UACA	GGC	100,000	102,000	0
GUCG	GGC	8,700	8,700	0
GCCG	GGC	16,000	3,000	122,000
GCUC	GGC	22,000	15,000	21,000
GGC	GGU	102,000	97,000	500
GGU	GGU	48,000	11,700	51,800
UGG	GGU	9,000	2,000	58,400
UACA	GGU	100,000	102,000	0
GUCG	GGU	8,700	8,900	0
GCUC	GGU	22,000	22,000	0

NOTE:  $K_b$  is the measured binding constant between the oligomer and tRNA<sup>Tyr</sup>.  $K_{obs}$  is the binding constant for the oligomer observed in the presence of the competitor; a reduction of the binding constant from  $K_b$  indicates competition.  $K_c$  is the binding constant of the competitor as computed by assuming equimolar competition for the same site. The experiments were conducted at 0°C.

SOURCE: After O. Uhlenbeck, *J. Mol. Biol.* 65:25 (1972).

Therefore, Equation 24-13 becomes

$$r_d = 1 + K_b(\text{tRNA})/[K_c(\text{Compet}) + 1] \quad (24-17)$$

The constant  $K_c$  can be measured by determining  $K_b$  as a function of the concentration of the competing oligomer. Table 24-3 summarizes such experiments for tRNA<sup>Tyr</sup>. In the simplest cases, the competition is a simple direct association with the binding site of the labeled oligomer. Then  $K_c$  is the same as the  $K_b$  that would be measured by directly studying the binding of the unlabeled competitor itself. Naturally, this is what is seen if unlabeled oligomer is used to compete with identical labeled oligomers.

Note from the results in Table 24-3 that GGU, which binds to the 3'-end of tRNA at A<sup>82</sup>C<sup>83</sup>C<sup>84</sup>, competes against the binding of UGG, which binds to an overlapping site, C<sup>83</sup>C<sup>84</sup>A<sup>85</sup>. Similarly, GGC (which binds to G<sup>18</sup>C<sup>19</sup>C<sup>20</sup> in the dihydrouridine loop) effectively competes against the oligomer GCCG (which binds to the overlapping site C<sup>16</sup>G<sup>17</sup>G<sup>18</sup>C<sup>19</sup>). However, what is especially interesting is that GGC also shows competition with GCUC, which binds to the nonoverlapping site G<sup>13</sup>A<sup>14</sup>G<sup>15</sup>C<sup>16</sup>. The fact that  $K_c$  for GGC in this competition is less than its  $K_b$

when measured alone suggests that both GGC and GCUC can bind simultaneously to the dihydrouridine loop, but that the binding of one weakens the affinity of the other. Neither GGC nor GGU affects the binding of any oligomers that associate with distant regions of the tRNA. This observation indicates that the binding is not triggering major conformational changes that are felt across the tRNA molecule, thus providing support for the validity of the technique.

Oligonucleotide-binding experiments have also been carried out on other tRNAs and on 5 S rRNA. For yeast tRNA<sup>Phe</sup>, the results are not as extensive as those for *E. coli* tRNA<sup>Tyr</sup>, but they are in general agreement. The results indicate that three regions are accessible for binding: the CCA end, the anticodon loop, and part of the dihydrouridine loop. The first two regions are in good agreement with expectations from the x-ray structure, which shows these regions as single strands. The third region is difficult to rationalize from the x-ray structure, but it is in reasonable agreement with the results obtained from slow tritium exchange (discussed earlier) and also from some chemical modification studies.

### Cross-linking and energy transfer

None of the methods we have discussed give a clear picture of the macroscopic organization of the tertiary structure of tRNA. They indicate which residues may be affected by tertiary-structure interactions, but one would like to know specifically how the loops and arms of the tRNA cloverleaf are folded to make up the tertiary structure. The only direct approach to answering this kind of question is to determine the spatial proximity of fixed points in the tRNA structure. Intramolecular cross-linking can provide proof that two residues are close, assuming that forming the cross-link does not perturb the tertiary structure.

Many *E. coli* tRNAs contain a 4-thiouridine in position 8 of the CCA stem. Near-UV irradiation of these tRNAs produces a photoadduct between the 4-thiouridine and cytidine-13 in good yield (Fig. 24-18a). The cross-linked material shows no significant perturbation in physical properties and is biologically active in a wide variety of different tests of tRNA function. Therefore, one can conclude that the CCA and dihydro-U stems in the tertiary structure of tRNA are folded such that positions 8 and 13 are immediately adjacent. This prediction is in complete accord with the tertiary structure of yeast tRNA<sup>Phe</sup> as revealed by x-ray crystallography (Fig. 24-18b). Note, however, that this tRNA species contains no 4-thiouridine, and so a direct test of the hypothesis is not possible. However, many lines of evidence indicate that almost all tRNAs have similar structures.

Cross-linking can yield information only about residues that are close to each other. Failure to observe a cross-link virtually never yields any useful information about the structure. A number of spectroscopic techniques are available for measuring proximity or remoteness, including various aspects of magnetic resonance and

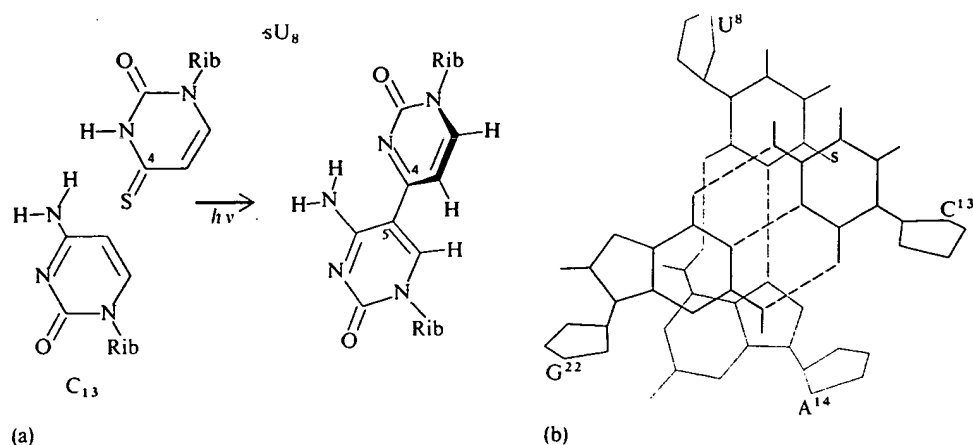


Figure 24-18

Cross-link formed by UV irradiation in many *E. coli* tRNAs. (a) Chemical structure of the cross-link between the 4-thiouridine in position 8 and the cytidine in position 13. [Courtesy of Nelson Leonard.] (b) Structure of adjacent A<sup>14</sup>-U<sup>8</sup> and C<sup>13</sup>-G<sup>22</sup> base pairs in the yeast tRNA<sup>Phe</sup> crystal structure, showing the proximity of residues 8 and 13. [After A. Rich and U.-L. RajBhandary, *Ann. Rev. Biochem.* 5:205 (1976).]

fluorescence-energy transfer. These techniques are discussed elsewhere in this book. Only the fluorescence technique has thus far been applied extensively to tRNA.

The first singlet energy-transfer experiments on tRNA by K. Beardsley and C. R. Cantor exploited the occurrence of the naturally fluorescent *Y* base adjacent to the anticodon of yeast tRNA<sup>Phe</sup>. Several different fluorescent dyes were attached covalently to the 3'-terminus of tRNA and served as energy acceptors. Only small amounts of energy transfer were seen in all cases, indicating that the 3'-end and the anticodon must be more than 40 Å apart. The consistency of results obtained with several different dyes served as assurance that some extreme value of  $\kappa^2$  (the geometric term in Eqn. 8-55) was not distorting the results.

Subsequently, D. Yang and D. Söll prepared a set of five samples of double-fluorescent labeled tRNAs. This was a much more difficult task, because both the donor and acceptor had to be put in by covalent chemical modification. Different tRNA species were used to construct different double-labeled samples, because the preparation of many of the covalent derivatives depended on the presence of particular unusual bases in the desired location and their absence at other locations. Figure 24-19 summarizes the results of energy-transfer measurements. If we assume that all tRNAs have identical tertiary structures (ignoring the "extra" loop), four of the five distance measurements available thus far agree fairly well with the crystal structure of yeast tRNA<sup>Phe</sup>. This is evidence that, at least in broad outline, the tertiary structure of

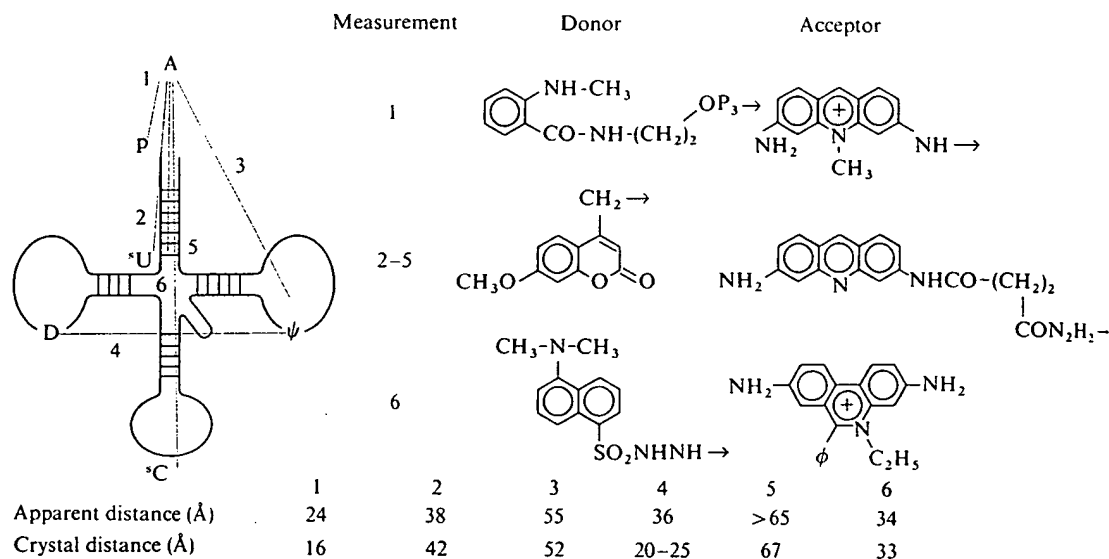


**Figure 24-19**

*Singlet-singlet energy-transfer measurements* compared with known distances within the yeast tRNA<sup>Phe</sup> crystal. Measurements 1 through 5 are from the work of Yang and Söll; measurement 6 is from Wells and Cantor. Most distances measured by energy transfer are in good agreement with the crystal distances. Because these measurements involved a number of different tRNAs, the results are a strong indication that all tRNAs can adopt very similar tertiary structures.

tRNA seen in the crystal must be the same as that occurring in aqueous solution. The energy-transfer results in Figure 24-19 are subject to some uncertainty, owing to lack of direct knowledge of  $\kappa^2$  (the average value of 2/3 was used), but the good agreement is circumstantial evidence that extreme  $\kappa^2$  values probably are not present.

Note that the results in Figure 24-19 are not detailed enough to allow an *a priori* determination of the geometric arrangement of the labeled regions. Dyes were placed in six positions on the tRNA: on the 3'- and 5'-ends, on the 4-thiouridine, and on bases in the anticodon, GT $\psi$ C, and dihydrouridine loops. Energy-transfer measurements provide scalar distances and not vectors. To compute the geometric structure of  $N$  points in space can require as many as  $4N - 10$  intramolecular distance ( $N \geq 4$ ). For the six covalently labeled positions in tRNA, this means that 14 of the 15 possible pairwise distances would be measured to define their geometric orientation. Five distances are far from sufficient. Even when all 14 are available, the structure determined is uncertain with respect to reflection in a mirror. Scalar distances are invariant to a mirror reflection, but an actual asymmetric structure is not. However, in concert with other available structural information, a few quantitative distance measurements



from energy transfer are quite informative, and they greatly restrict the range of plausible tertiary structures warranting further consideration.

Energy transfer also can be used to locate the sites of interaction of other molecules with tRNA. For example, in the presence of sufficient  $Mg^{2+}$  to ensure that tRNA is in the native tertiary structure, there is a single strong binding site for ethidium. This bound ethidium was used by B. Wells and Cantor as an energy acceptor for a dye attached at the 3'-end, yielding a distance of 34 Å between the dyes. An examination of the tRNA<sup>Phe</sup> tertiary structure reveals that the only plausible double-strand binding site located this distance from the 3'-end is between residues 6 and 7 (Fig. 24-19). X-ray and NMR studies are consistent with this assignment, but the former yield the unexpected result that the bound ethidium is not intercalated.

### A phase diagram for tRNA conformations

As environmental conditions are varied, tRNAs can assume a range of structures. Among the environmental variables thus far studied extensively are monovalent ion concentration, temperature, divalent ion concentration, and pH. One rationale for examining structural changes induced by alterations in conditions is that these may reflect possible conformational changes linked to tRNA function when it complexes with aminoacyl synthetases, protein synthesis factors, or the ribosome. It is far easier to examine the conformations of isolated tRNA than to study much larger nucleoprotein complexes. Studies of the tRNA conformational changes also can lead to increased knowledge about the forces that stabilize the native structure of tRNA. Furthermore, such studies can provide a framework for planning structural studies on more complex RNAs for which high-resolution x-ray or NMR data currently are unavailable.

We concentrate here on the effects of monovalent ions and temperature, because there are fairly comprehensive results for these two variables. A single tRNA, *E. coli* tRNA<sup>Met</sup>, will be used to demonstrate how conformational changes have been resolved and analyzed. Available results for other tRNAs are qualitatively similar but differ in a number of important details. It is conceivable that such differences are functionally important because tRNA<sup>Met</sup> is responsible for initiating protein synthesis but, unlike any other tRNA, it is not involved in protein chain elongation. However, the only obvious secondary-structure difference between tRNA<sup>Met</sup> and other tRNAs is one missing base pair at the end of the CCA stem (Fig. 3-7). From the known tertiary structure of yeast tRNA<sup>Phe</sup>, it is not obvious that a broken base pair at this position should perturb any other region of the structure. L. Schulman has shown that chemical modifications allowing base-pair formation at the end of the CCA stem of *E. coli* tRNA<sup>Met</sup> render the tRNA able to participate in many of the protein-synthesis functions of normal tRNAs. Thus, it seems likely that the following results are not particularly related to the specialized role of tRNA<sup>Met</sup>.

The first objective is to define the critical values of temperature and  $\text{Na}^+$  concentration at which major conformational changes occur. The absorbance at 260 nm traditionally has been used to monitor RNA conformational changes. For *E. coli*  $\text{tRNA}_{\text{f}}^{\text{Met}}$ , it proved very useful to supplement such data with absorbance measurements at 335 nm. These data almost exclusively reflect the environment of the 4-thiouridine residue in position 8. Discrete conformational changes are easier to resolve at this wavelength, because thermal melting at this wavelength is clearly biphasic (Fig. 24-20). Data at 260 nm also show evidence of biphasic melting, but

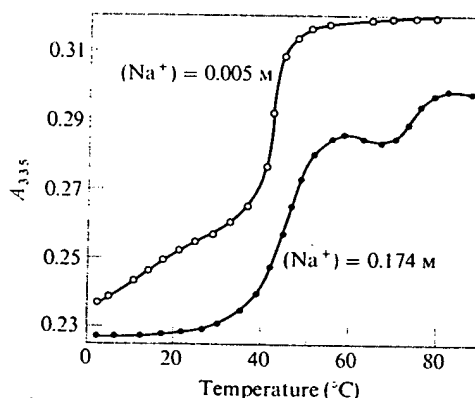


Figure 24-20

Absorbance melting of *E. coli*  $\text{tRNA}_{\text{f}}^{\text{Met}}$  monitored at 335 nm and measured at two different salt concentrations. This wavelength essentially follows only 4-thiouridine absorbance and appears to be more sensitive than 260 nm to tertiary structure changes. [After P. E. Cole et al., *Biochemistry* 11:4358 (1972).]

it is more difficult to resolve because the transition with a lower  $T_m$  involves a rather small absorbance change. The 4-thioU is not involved in any cloverleaf duplex region, but it clearly is involved in tertiary structure. Thus, the very large 335 nm low-temperature absorption transition immediately suggests a tertiary-structure alteration.

From thermal-melting studies at a variety of ionic strengths, it is possible to construct a phase diagram for  $\text{tRNA}_{\text{f}}^{\text{Met}}$  as described in Chapter 22 for poly A·U (Fig. 24-21). There is evidence for four phases in the absence of  $\text{Mg}^{2+}$ . The low-temperature, high-ionic-strength form (I) almost certainly is tRNA in its native tertiary structure. Addition of  $\text{Mg}^{2+}$ , known to stabilize the native structure, has very little effect on the absorption properties of tRNA in this region. The hypochromicity of the high-temperature, low-ionic-strength form (IV) is close to zero. Thus, this form is essentially a single-stranded coil. The exact position of the phase boundary between the other two forms (II and III) is not well defined by available experimental results. It is easy to see why; direct II  $\leftrightarrow$  III interconversion is not

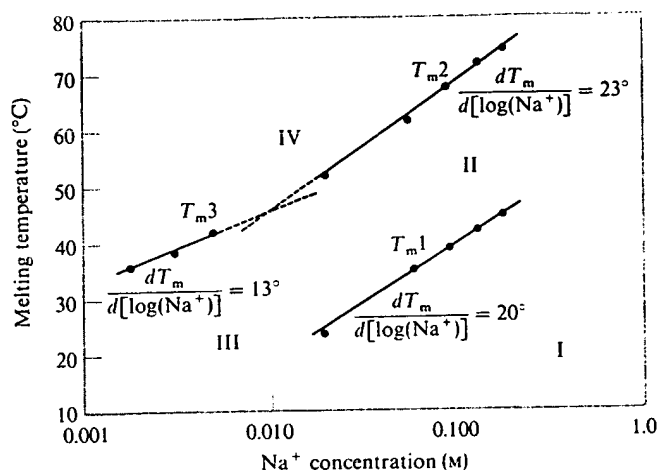


Figure 24-21

Phase diagram for *E. coli*  $tRNA^{\text{Met}}$  at neutral pH. This diagram was constructed from the results of melting experiments like that shown in Figure 24-20 and is supported by the results of kinetic studies. See Figure 24-22 for a pictorial representation of the structures of tRNA in the four phases. [After P. E. Cole et al., *Biochemistry* 11:4358 (1972).]

resolved in thermal melting at constant salt concentration. In principle, one should be able to study the  $\text{II} \leftrightarrow \text{III}$  transition by varying the sodium ion concentration. However, the optical change for the  $\text{II} \leftrightarrow \text{III}$  transition is too small to work with conveniently, as you may be able to infer from Figure 24-21.

#### Relaxation kinetics of tRNA conformational changes

Several lines of evidence suggest that zones II and III in Figure 24-21 correspond to different tRNA conformations. The slopes of the II–IV and III–IV phase boundaries,  $dT_m/d[\log(\text{Na}^+)]$ , differ by almost a factor of two. The lower slope of the III–IV boundary suggests that the  $\text{Na}^+$  binding is less important in stabilizing form III than form II. This observation is consistent with the fact that III is favored over II at low salt concentration and constant temperature. Stronger evidence is provided by kinetic studies. The process  $\text{III} \rightarrow \text{I}$  has been monitored by rapidly increasing the  $\text{Na}^+$  ion concentration and following absorbance changes. A very slow first-order rate is seen with a relaxation time of 1,200 sec at 13.3°C. The activation energy for this process is 61 kcal mole<sup>-1</sup>, a very large value. This long relaxation effect helps to locate the  $\text{I} \rightarrow \text{III}$  boundary at salt concentrations too low to resolve the entire I–III melting transition.

The rate of the  $\text{I} \leftrightarrow \text{II}$  transition must be studied by temperature-jump relaxation

kinetics, because it is too fast for salt-jump techniques. At the lowest temperatures at which the process can be observed, the relaxation time  $\tau$  for this transition is about 7 msec and is temperature-independent, implying a zero activation energy. At higher temperature,  $\tau$  becomes markedly temperature-dependent, and an apparent activation energy of 50 kcal mole<sup>-1</sup> can be derived from the data. The great difference in rates between the I  $\leftrightarrow$  III and I  $\leftrightarrow$  II transitions implies that states II and III are quite different entities. P. E. Cole and D. M. Crothers showed that the activation energies of various steps are particularly informative. For the I  $\leftrightarrow$  II relaxation kinetics, the single  $\tau$  observed must be  $\tau^{-1} = k_{I \rightarrow II} + k_{II \rightarrow I}$ . At temperatures well below the  $T_m$  for the transition,  $k_{II \rightarrow I} \gg k_{I \rightarrow II}$  and, therefore, the zero activation energy observed must correspond to II  $\rightarrow$  I. Conversely,  $k_{I \rightarrow II}$  is completely dominant above  $T_m$ , and so its activation energy must be about 50 kcal mole<sup>-1</sup>. Because form II can convert to I with no activation energy, no significant interactions within II are disrupted in order to produce I. Therefore, it is likely that form II has lost some of the tertiary or secondary interactions present in native tRNA I, but has not gained any new ones.

The rate of the I  $\leftrightarrow$  II interconversion is orders of magnitude too slow for the melting of a simple hairpin, which we have shown to occur in microseconds. Therefore, some tertiary-structure changes must be involved. However, the large activation energy for  $k_{I \rightarrow II}$  seems difficult to rationalize on the basis of tertiary structure alone, and so it seems reasonable to postulate that the conformational change involves additional loss of some secondary structure and thus large enthalpy changes. A tentative assignment suggests that the I  $\rightarrow$  II transition involves loss of all tertiary structure and melting of the dihydrouridine loop (Fig. 24-22). From the energetics of RNA conformations discussed earlier, region II is predicted to be the least stable secondary-structure region.

The large activation energy of the III  $\rightarrow$  I transition shows that this must be a process very different from II  $\rightarrow$  I. Specifically, quite a few base-base interactions must be present in III that are not present in I, and these must be broken for the conformational change to occur. A reasonable guess is that form III is a hairpinlike structure (Fig. 24-22). This extended structure would have lower electrostatic free energy than the cloverleaf or native tRNA tertiary structure. Thus it could be more stable at low ionic strengths. Hydrodynamic data on tRNA at very low salt concentration are consistent with an elongated conformation.

The conformational change II  $\rightarrow$  IV appears simple when observed by equilibrium thermal melting, but relaxation kinetic studies show otherwise. Three distinct relaxation processes are seen in the temperature range corresponding to this transition. These can be resolved because, although they take place in overlapping temperature ranges, they occur on quite different time scales. The results shown in Figure 24-23 demonstrate the power of kinetics to elucidate conformational changes. However, they also highlight a major limitation. The individual relaxation steps generally cannot be assigned to particular processes unless considerable additional information is available from higher-resolution structural techniques.

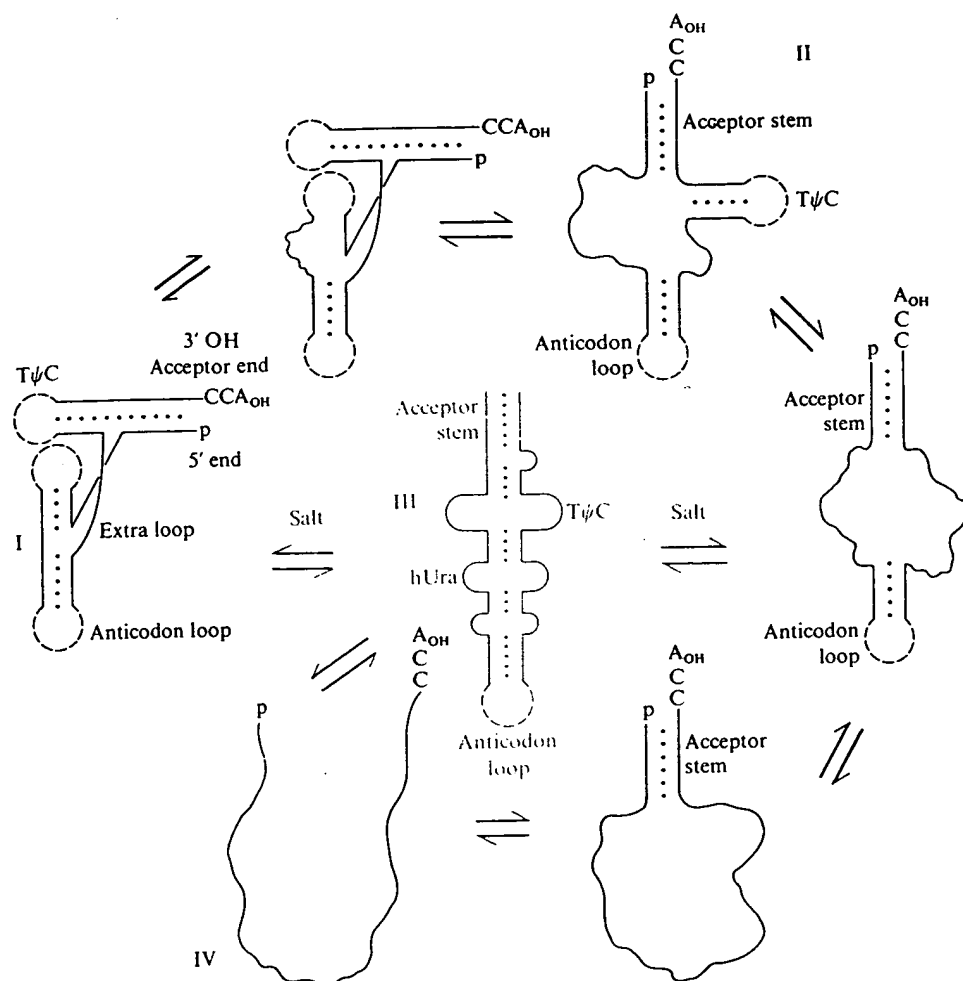


**Figure 24-22**

Schematic of thermal melting of *E. coli* tRNA<sup>Met</sup>. The order in which various regions of structure are disrupted was established from the NMR and kinetic studies shown in Figure 24-23. Also indicated are the four states (I through IV) believed to correspond to regions of the phase diagram for this tRNA shown in Figure 24-21. The form of tRNA stable only at low salt and low temperature (III) is shown in color. [After D. M. Crothers et al., *J. Mol. Biol.* 87:63 (1974).]

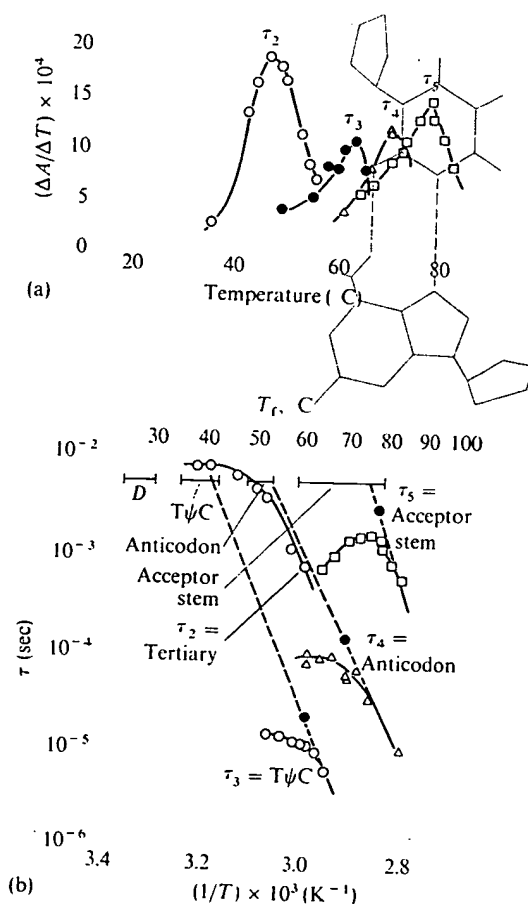


**Figure 24-23**

Thermal unfolding studies of *E. coli* tRNA<sup>Met</sup> in 0.17 M Na<sup>+</sup>. (a) Differential thermal transition profiles for four discrete relaxation kinetic steps.  $\Delta A / \Delta T$  is the amplitude of total absorbance change for each step, normalized by the size of the temperature jump employed. The different steps can be resolved so well because they occur on very different time scales, even though they overlap in temperature range. (b) Variation of four relaxation times with temperature. At the top are indicated the temperature ranges at which NMR melting of each region is observed. These ranges are plotted on the time scale at the characteristic NMR times for exchange broadening (see text). Also shown are the four relaxation processes seen by temperature-jump absorbance measurements. All points are directly measured, except for the dark ones, which were obtained from the fact that each  $2\tau = 1/K_{-i}$  at  $T = T_m$ . Note the excellent extrapolation of the temperature-jump results to the NMR results. [After D. M. Crothers et al., *J. Mol. Biol.* 87:63 (1974).]

### ● Using NMR measurements to assign relaxation values

The proton NMR spectrum of tRNA<sup>Met</sup> was studied under the same sets of conditions used for relaxation kinetics. As the temperature of the tRNA sample is raised, selective broadening occurs of specific sets of low-field N-H...N proton resonances. For example, between 21° and 37°C, the integrated intensity of the NMR spectrum decreases by approximately four resonances. Two of these clearly are resolved single-proton peaks at -13.65 ppm and -11.45 ppm, and these can be assigned tentatively to A<sup>11</sup>-U<sup>26</sup> and G<sup>10</sup>-C<sup>27</sup>, respectively, as discussed earlier. Because both of these pairs are in the dihydrouridine stem, it is reasonable to conclude that this whole stem is melting concertedly, and the locations of the other two resonances that disappear are consistent with this. In a similar way, the melting regions of the TψC, anticodon, and acceptor stems can be assigned at successively higher temperatures (Fig. 24-23b).

To make the connection between an NMR melting temperature and an optical relaxation time, one must take into consideration the different time scales implicit in the two techniques. An NMR spectrum will broaden when exchange of the protons involved becomes comparable to NMR characteristic times. The situation is potentially quite complicated because two different processes can lead to broadening for the *i*th duplex region. The first process is duplex opening:



The second process is solvent exchange:



The rates seen optically are  $k_i$  and  $k_{-i}$ , whereas NMR could be monitoring these or  $k_{ex}$  and  $k_{-ex}$  or both sets of rates.

Some limiting cases allow a simple interpretation. Suppose that duplex opening is slow on the NMR time scale, but solvent exchange is fast once single strands are formed. Then it can be shown that  $k_{-i}$  determines the line broadening of the duplex resonances seen at -11 to -15 ppm. When duplex opening and solvent exchange both are slow,  $k_{-i}$  again dominates. If both processes are fast, then the relaxation time  $\tau$  of the duplex transition becomes important:  $\tau^{-1} = k_i + k_{-i}$ . When  $k_{ex}\tau \gg 1$ , exchange with water occurs virtually every time the helix is open, and it can be shown that  $k_{-i}$  still dominates the line width. However, where  $k_{ex}\tau \ll 1$ , the solvent exchange dominates. We shall assume that this last case is not applicable to any of the tRNA data.

The measured optical relaxation data yield a value of  $k_{-i}$ . At high temperatures, this value must dominate the observed relaxation time  $\tau_{opt}^{-1} = k_i + k_{-i}$  because, at the high-temperature part of each optical melting transition,  $k_{-i} \gg k_i$ . However,

optical melting occurs on a time scale much faster than that required to cause NMR broadening. Hence, one must extrapolate the measured  $k_{-i}$  values back to the NMR time scale. It was found, from measurements on model oligonucleotide duplexes, that a choice of  $\tau_{\text{NMR}} = 5$  msec brings melting curves measured by NMR and by optical techniques into coincidence. Figure 24-23b shows the NMR melting regions on this time scale. You can see that a rather long extrapolation of the optical data is required. One can construct an additional data reference point to increase reliability at lower temperatures by realizing that  $k_i = k_{-i}$  at the optical  $T_m$ , and so each  $\tau_{\text{opt}}^{-1} = 2k_i$  at  $T_m$ . The three high-temperature relaxation times extrapolate beautifully back to each one of the NMR melting transitions (Fig. 24-23b). Thus each optical transition is assigned.

#### Steps in the melting of tRNA

Figure 24-22 shows the detailed steps in the thermal melting of tRNA<sup>Met</sup>, corresponding to processes I  $\rightarrow$  II and II  $\rightarrow$  IV of the phase diagram. Let us see how these steps can be rationalized. No separate optical melting was seen for the dihydrouridine helix or the tertiary structure. However, NMR clearly showed that the dihydrouridine-stem protons can exchange at a low temperature. Thus, it appears that a small degree of transient opening of this helix can occur prior to its actual thermal melting, which coincides with loss of tertiary structure. From the duplex interaction energies of Table 23-4, the T $\psi$ C stem is predicted to be the next least stable helix after the dihydrouridine stem, and this is in accord with the assignments of Figure 24-23.

The highest-temperature optical melting transition is assigned to the acceptor-stem duplex. Note that this transition has the slowest relaxation time of any of the three, due solely to secondary structure. This is quite reasonable. Below its  $T_m$ , when the rate of helix formation dominates the relaxation kinetics, the relaxation time should be small, because the improbability of closing such a large loop will strongly inhibit the reaction. Note the unusual temperature dependence of this transition (Fig. 24-23). The relaxation time decreases below  $T_m$  as well as above  $T_m$ . The former effect probably is due to coupling between melting of the acceptor stem and of the anticodon stem.

We have been discussing each transition as though it were unaffected by all the others, but this clearly is an oversimplification. The acceptor-stem and anticodon-stem meltings overlap in temperature range. When the anticodon stem is partially duplex, it must speed the rate of formation of the acceptor stem, because the size of the loop required to close the acceptor stem becomes substantially reduced. It actually is surprising that more coupling effects are not seen. However, it also is fortunate, because severe coupling can lead to new relaxation times that are functions of several of the fundamental duplex times, and this effect can severely inhibit any attempt to assign and analyze each optical relaxation.



Note that the two duplex regions that turn out to be most stable in thermal melting are also the two postulated to remain intact when tRNA is converted into an elongated form at low salt concentration. In contrast, the relatively easy melting of the tertiary structure and of the dihydrouridine stem suggest that, in the various functional roles of tRNA, these two regions probably could undergo conformational changes. It is important to recognize from the studies of tRNA melting we have summarized how the different experimental techniques gain in strength when used in concert. NMR permitted indirect assignments of optical melting transitions to be confirmed, and the optical melting studies strengthened confidence in the assignments of particular resonances in the NMR spectrum. This symbiosis of various techniques is likely to be a necessity if the conformational equilibria and dynamics of some of the more complex RNAs ever are to be understood.

### Secondary and tertiary structure of large RNAs

As an example of what the future has in store, consider the partial sequence of bacteriophage MS2 RNA in Figure 24-24. This sequence has been folded into a secondary structure locally consistent with the known duplex and loop interactions; but with such a large sequence (as with a typical protein), there is no practical way to examine all possible base-pairing schemes to be sure that a globally most-stable secondary structure has been found. Some aspects of the MS2 RNA secondary structure surely are important for function, and uncovering these aspects is a major challenge.

Techniques for the exploration of the structure of large RNAs are still in their infancy. One approach that appears to have considerable promise is intramolecular RNA cross-linking. For example, various psoralen derivatives bind specifically to double stranded regions and produce cross-linking efficiently upon UV irradiation. Other reagents appear able to cross-link specifically between two nearby single-stranded regions or between two nearby double-stranded regions. The approximate location of cross-links is found by examining the RNA in the electron microscope after vigorous denaturation. Molecules without cross-links appear as extended rods, whereas those with cross-links contain loops. Measuring the loop location reveals the approximate position of the cross-link. In ideal cases, an exact cross-link position should be accessible by rapid gel sequencing techniques.

A fundamental question about RNA structure is the relative potential for forming base pairs between residues nearby in the sequence (hairpins) versus those between residues far apart in the sequence (loops). The former are more favorable when the local thermodynamics are considered, but the cost in free energy of closing a large loop is really not that great and can easily be compensated for by a few G-C pairs. In preliminary studies on rRNA, numerous double-stranded interactions producing large cross-linked loops have been seen. However, the overall balance between hairpins and loops remains to be proven.

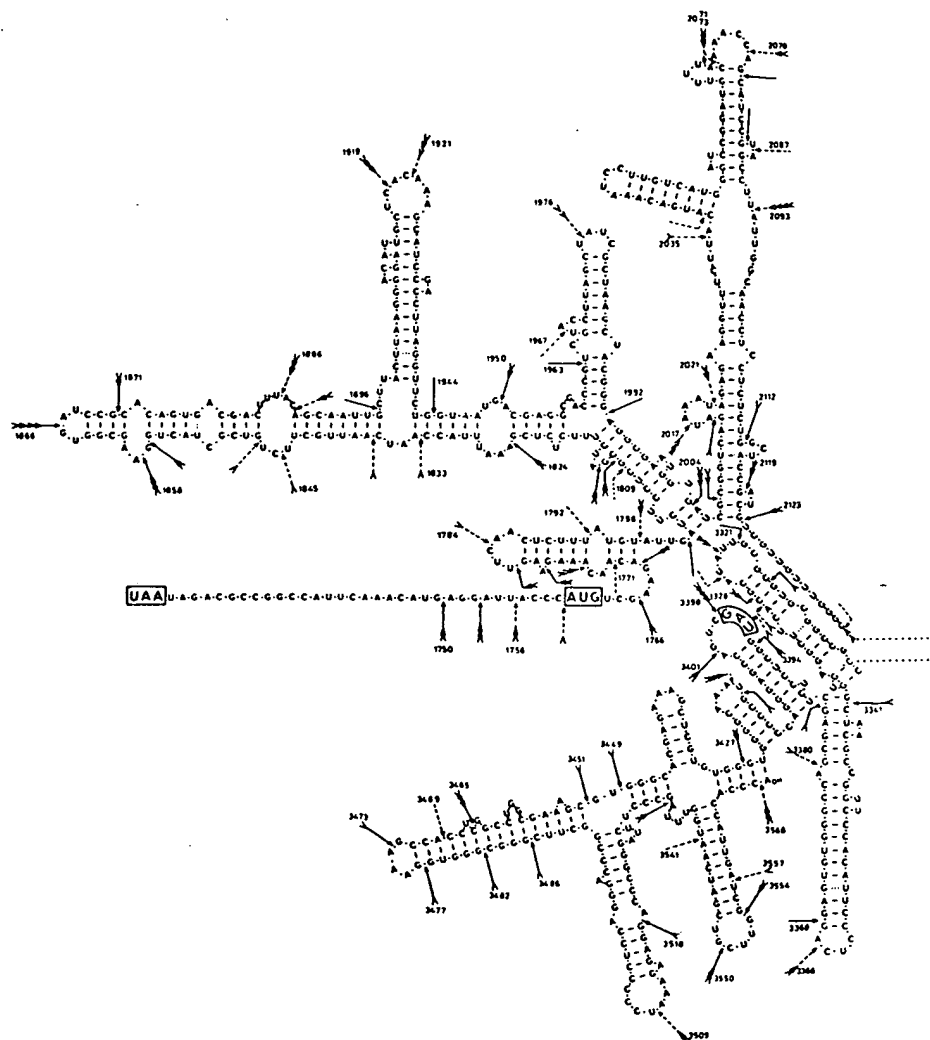
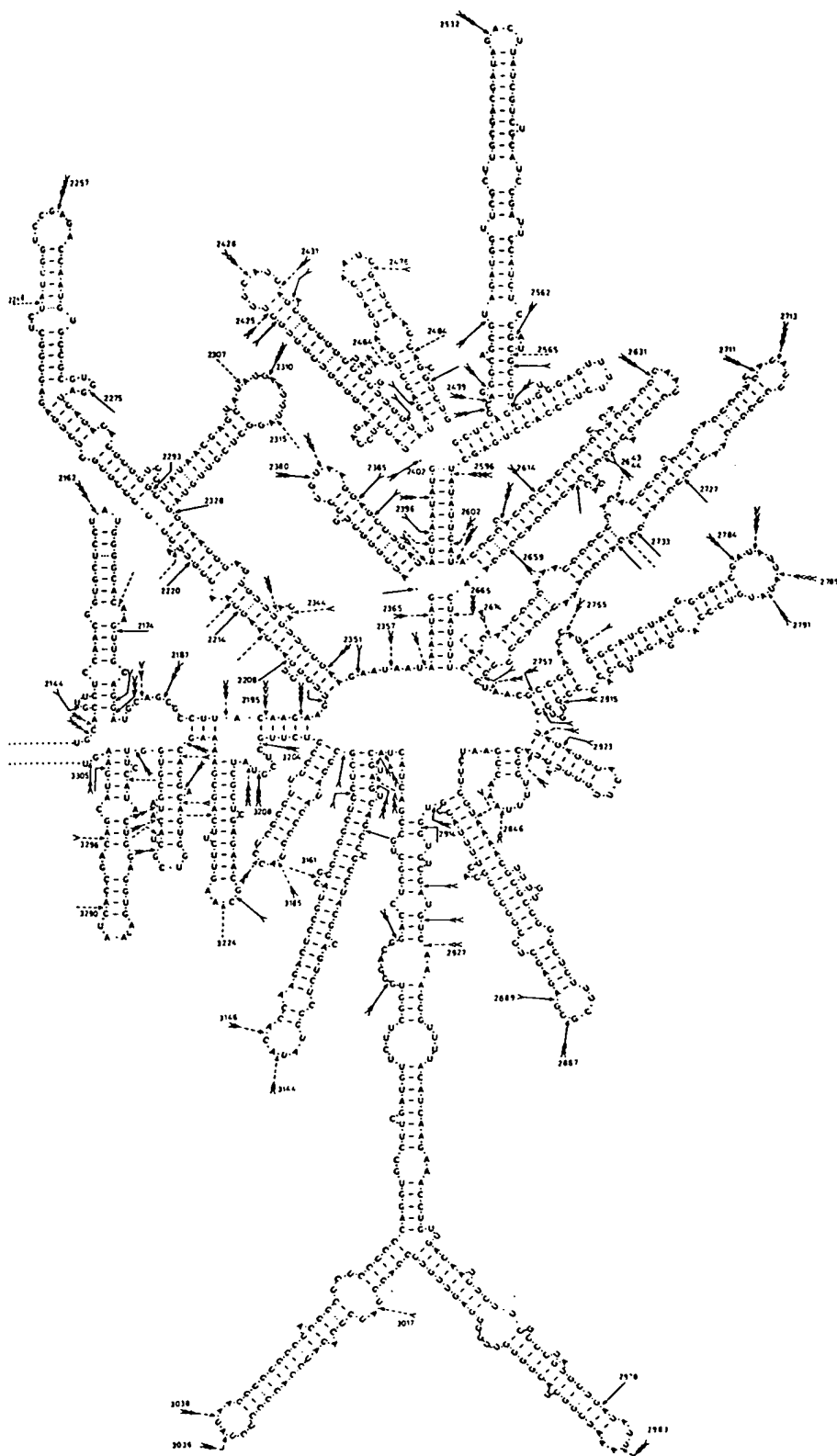


**Figure 24-24**

Part of the sequence of MS2 RNA, folded into a plausible secondary structure using (locally) the energy considerations of Tables 23-4 and 23-5. Arrows point to sites easily split by nucleases during partial digestion. [After W. Fiers et al., *Nature* 260:500 (1976).]



### Summary

A topological constraint exists in closed circular duplex DNA. The linking number (the number of times one strand passes through the circle formed by the other) must remain constant. This leads to a coupling between the number of local helix turns (or the parameters characterizing a local helix) and the tendency of the DNA to coil into superhelices. Naturally occurring DNA closed circles appear to have negative toroidal superhelices. Adding an intercalating agent such as ethidium will progressively remove these superhelices to produce a relaxed DNA duplex circle. Further binding of ethidium leads to the incorporating of positive toroidal turns in the DNA. From a knowledge of the unwinding angle accompanying the binding of a single ethidium, it is possible to compute the average number of supercoils present in a DNA sample. DNAs with identical molecular weight but different supercoil number can be physically separated by gel electrophoresis. Supercoiling provides an extremely sensitive tool for monitoring local structural changes in DNA because it amplifies these into gross structural changes.

RNA tertiary structure in solution has been studied most extensively in tRNA. Spectroscopic techniques can provide estimates of the extent of base pairing. NMR appears capable in many cases of determining which particular residues are base-paired. Sequences that remain exposed or single-stranded can be identified by purine  $C^8$ -tritium exchange and by their ability to bind complementary oligonucleotides. The overall pattern of folding of individual helix stems and loops can be assessed by cross-linking and by singlet-singlet energy-transfer techniques. Various conformations become accessible to tRNAs as the salt concentration and temperature are raised. Combining equilibrium melting and kinetic studies allows construction of a phase diagram for tRNA structures. The detailed stages in tRNA melting can be analyzed by examining the temperature dependence of the NMR spectrum and then correlating the disappearance of sets of base-paired residues with relaxation times visible by temperature-jump kinetics.

**This Page is Inserted by IFW Indexing and Scanning  
Operations and is not part of the Official Record**

**BEST AVAILABLE IMAGES**

Defective images within this document are accurate representations of the original documents submitted by the applicant.

Defects in the images include but are not limited to the items checked:

☒ **BLACK BORDERS**

☐ **IMAGE CUT OFF AT TOP, BOTTOM OR SIDES**

☒ **FADED TEXT OR DRAWING**

☐ **BLURRED OR ILLEGIBLE TEXT OR DRAWING**

☐ **SKEWED/SLANTED IMAGES**

☐ **COLOR OR BLACK AND WHITE PHOTOGRAPHS**

☐ **GRAY SCALE DOCUMENTS**

☐ **LINES OR MARKS ON ORIGINAL DOCUMENT**

☐ **REFERENCE(S) OR EXHIBIT(S) SUBMITTED ARE POOR QUALITY**

☐ **OTHER:** \_\_\_\_\_

**IMAGES ARE BEST AVAILABLE COPY.**

**As rescanning these documents will not correct the image problems checked, please do not report these problems to the IFW Image Problem Mailbox.**